The impact of high hydrostatic pressure maintenance after high-pressure torsion on phenomena during high hydrostatic pressure annealing

Krawczynska, A. T.; Kerber, M.; Suchecki, P.; Romelczyk-Baishya, B.; Liedke, M. O.; Butterling, M.; Hirschmann, E.; Wagner, A.; Lewandowska, M.; Setman, D.;

Originally published:

April 2022

Materials Science and Engineering A 840(2022), 142874

DOI: https://doi.org/10.1016/j.msea.2022.142874

Various routes of high hydrostatic pressure annealing of nanostructured nickel

Agnieszka Teresa Krawczynska*[1], Michael Kerber[2], Przemyslaw Suchecki[1], Barbara Romelczyk-Baishya[1], Maciej Oskar Liedke[3], Maik Butterling[3], Eric Hirschmann[3], Andreas Wagner[3], Malgorzata Lewandowska[1], Daria Setman[2]

[1] *Warsaw University of Technology, Faculty of Materials Science and Engineering, Woloska 141, 02-507 Warsaw, Poland*

[2] *University of Vienna, Faculty of Physics, Boltzmanngasse 5, A-1090, Vienna, Austria*

[3] *Institute of Radiation Physics, Helmholtz-Zentrum Dresden – Rossendorf, Bautzner Landstraße 400, 01328 Dresden, Germany*

*agnieszka.krawczynska@pw.edu.pl, tel. +48 22 234 81 55, fax. +48 22 234 85 14

michael.kerber@univie.ac.at
przemyslaw.suchecki@gmail.com
bromelczyk@gmail.com
m.liedke@hzdr.de
m.butterling@hzdr.de
a.wagner@hzdr.de
e.hirschmann@hzdr.de
malgorzata.lewandowska@pw.edu.pl
daria.setman@univie.ac.at

Abstract

The impact of high hydrostatic pressure release after high-pressure torsion on subsequent high hydrostatic pressure annealing was analyzed by performing experiments on nanostructured Ni. Ni was deformed by high-pressure torsion at a pressure of 6GPa in 5 turns. Directly after deformation, the pressure was reduced to 2GPa, and under 2GPa annealing at 400°C was conducted for 5 min. For comparison, samples were also annealed under 2GPa after deformation without loading between processes. Microhardness measurements, detailed microscopy observations and positron annihilation spectroscopy investigations were performed to elucidate the changes in the microstructures obtained after different processing routes. It is demonstrated that the pressure applied between deformation and high hydrostatic

pressure annealing caused an increase in microhardness by 20% in comparison with pressure realize. Moreover, the pressure applied had an impact on the vacancy concentration, and consequently on the microstructure, leading to a smaller average grain size and a more heterogenous microstructure in terms of grain size, leaving space for optimizing the strength-ductility balance.

Keywords: nanomaterials, high pressure torsion, annealing, positron annihilation, defects

1. Introduction

Severe plastic deformation (SPD) processing leads to the generation and storage of lattice defects such as vacancies and dislocations [1-3]. For relatively low strains, dislocation cell structures are created, and with increasing strain dislocations rearrange to form grain boundaries, including those of a non-equilibrium character [4]. The increase in dislocation density is accompanied by an increase in vacancy concentration. The defects introduced by SPD are essential, since they are responsible for unique mechanical and physical properties of SPD-processed materials.

The density of dislocations, which may reach an order of 10^{15} m^{-2} with an increasing number of passes in SPD, has been studied extensively using transmission electron microscopy [5,6]. However, the investigation of vacancies demands a more complex approach. For instance, a combined evaluation using X-ray line profile analyses, differential scanning calorimetry and residual electrical densitometry was used to reveal that, in the case of equal channel angular processed (ECAP) Cu - route B_c, a strongly enhanced concentration of vacancies is achieved in comparison with conventional deformation performed to a similar degree of deformation [7]. Similar investigations were performed on high-pressure torsion (HPT) processed Ni and Cu. They proved that, in HPT-processed Ni, in comparison with Cu the total maximum concentration of vacancies considering both agglomerates and single/double vacancies is higher. Moreover, single/double vacancies were observed in Ni, whereas in Cu only vacancy agglomerates were present [8]. It is highly probable that materials having a lower stacking fault energy (SFE) may be prone to form vacancy agglomerates. Moreover, the generation of a high density of vacancies in HPT-processed Cu was also proved by positron annihilation spectroscopy [9, 10]. Vacancy agglomerates of 4–5 vacancies were found in the center of the disc, and of 7-9 at the periphery. Generated vacancies play an important role during the

annealing of SPD-processed materials, as the rapid release of excess vacancies in the early stage of heat treatment is responsible for accelerated atomic mobility. Vacancies also govern the annihilation of edge dislocations by climbing. Moreover, the hardening by annealing effect arises from an agglomeration of deformation-induced vacancies [11].

Under the increased pressure during SPD processes, extra work must be applied to enable vacancies to migrate through the lattice. Consequently, the effective vacancy migration enthalpy increases, leading to a lower diffusion coefficient [12]. It was revealed by in situ X-ray diffraction experiments with the application of cooling of the anvils confining the sample after stopping deformation [13-15] that the size of the coherently scattering domains is not strongly affected by the pressure release, whereas the dislocation density decreases drastically in the case of HPT-processed Cu. This phenomenon is observed to a lesser extent in HPT-processed Ni due to its higher activation enthalpy [14, 15]. Moreover, in situ X-ray line profile analysis using synchrotron radiation proved for HPT-processed Ni that the higher the pressure applied during HPT, the higher the dislocation density and the earlier and more profound the annihilation of dislocations during pressure release [13].

Such changes in defect characteristics during high hydrostatic pressure release may have a major impact on the processes taking place during annealing, especially if the annealing is conducted under high hydrostatic pressure (HPA). During HPA, the movement of vacancies is made difficult, as are diffusion-govern processes. The annihilation of vacancies is hindered, since high hydrostatic pressure has an impact on vacancy migration. Consequently, vacancy migration influences the annihilation of edge dislocations climbing and the microstructure transformation, as has been proved in previous HPA experiments [16-27]. These have shown that HPA hindered grain growth. However, the greater the deformation degree, the faster the grain growth under high hydrostatic pressure, as observed in conventionally deformed and HPT-processed austenitic stainless steel, which differed in the equivalent strain applied during deformation, after annealing at 900°C for 10 min at 2 and 6GPa [22]. Moreover, grain growth strongly depends on SFE [27]. It has been proved that factors such as higher vacancy concentration and lower deformation twins density were responsible for faster grain growth during HPA in Ni than in Ag of 125 and 16 mJ/m^{-2} SFE, respectively [28]. Additionally, HPA had an impact on the volume fraction of high-angle grain boundaries, as it contributed to hindering the movement/creation of low-angle grain boundaries in HPT-processed austenitic

stainless steel. Low-angle grain boundaries are well-ordered and can migrate only by the vacancy migration mechanism [20]. This mechanism is made difficult during HPA.

Therefore, this work was initiated in order to determine the impact of the pressure applied between HPT and HPA on the microstructure and mechanical properties after HPA in comparison with the pressure release. It is important to underline that these modifications - pressure presence and release between deformation and high hydrostatic pressure annealing - have been applied for the first time in high hydrostatic pressure annealing experiments. It was only possible thanks to the application of high hydrostatic pressure device. A second goal was to evaluate the possibility of controlling grain size to achieve a better strength-plasticity balance, which is one of the most fundamental issues and long-standing conflicts in materials science and engineering.

2. Experimental

2.1 Materials and experiments

In the present study, Ni of 99.99% purity was investigated. From Ni bars, disks of 0.8 mm in thickness and 10 mm in perimeter were cut by spark erosion; the disks were then annealed at 600°C for 2 h in order to obtain a well-recrystallized microstructure. The HPT experiments were carried out at the Faculty of Physics at the University of Vienna. The disks were HPT-processed at a pressure of 6GPa and a speed of 0.2 rpm up to 5 revolutions. The strain was well defined as simple shear, γ, and was calculated according to the equation $\gamma = 2\pi \times r \times n/t$, where r, n and t are the distance from the torsion axes, the number of applied revolutions and the mean thickness of the sample, respectively. The equivalent strains $\varepsilon_{eq} = \gamma/\sqrt{3}$, calculated at 3.5 mm from the central point of the sample after 5 revolutions, were equal to 79. After deformation with a decrease in pressure to 2GPa or with a complete unloading, the samples were annealed at 400°C under a pressure of 2GPa in an HPT device for 10 min. The heating and cooling rates during high hydrostatic pressure annealing were 1200 and 50°C/min, respectively. The selection of experimental conditions was based on previous experiments [27]. Schematically the experiment is presented in **Fig. 1**. Further on in this text, this annealing technique is referred to as HPA – high hydrostatic pressure annealing, and the samples are referred to as Ni_HPT – after HPT, Ni_HPT_L_HPA – after HPT additional pressure and HPA and Ni_HPT_U_HPA – after HPT unloading and HPA. The reference sample after conventional annealing at 600°C for 2h is referred to as Ni_A.

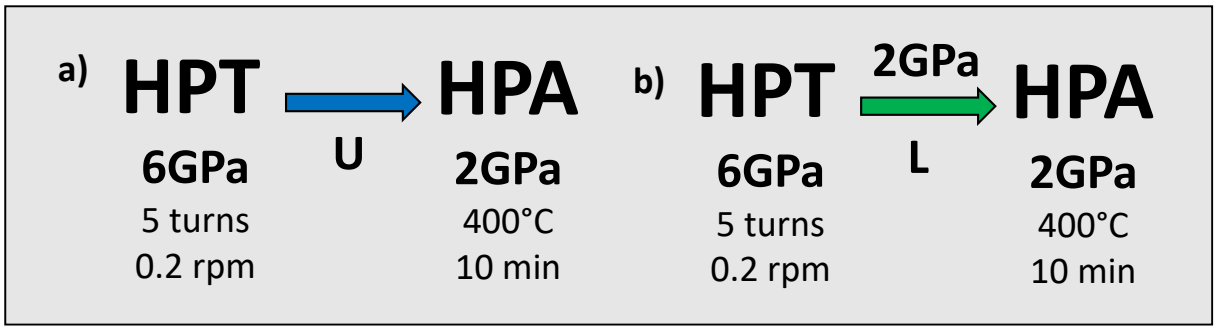

Fig. 1 Scheme of various routes of HPT and HPA experiments a) with pressure release between HPT and HPA - unloaded, b) with pressure between HPT and HPA - loaded

2.2 Analysis methods

a) Microhardness measurements

After conventional annealing, HPT and HPT combined with HPA, microhardness was measured using an MHT-4 microhardness tester manufactured by Paar equipped with a Zeiss microscope. The indentation force was 1N, the rate 0.1N/s and the holding time 10 s. The indentations were performed on the diameter, with a distance of 0.5 mm between them.

a) Variable energy positron annihilation lifetime spectroscopy

For variable energy positron annihilation lifetime spectroscopy (VEPALS) measurements, the samples after HPT, combined HPT and HPA were polished under a conventional mechanical polishing procedure (firstly with a diamond suspension containing particles of 3 μm in diameter under a load of 15 N for 10 min and subsequently with diamond particles of 1μm in diameter under a load of 10 N for 10 min). Afterwards, polishing by vibrating polishing using a Buehler Vibromet in an amorphous colloidal silica suspension for 3 h was performed to remove defects introduced by conventional polishing. The VEPALS measurements were conducted at the Mono-energetic Positron Source (MePS) beamline at HZDR, Germany [29,30]. The beam size was approximately 5 mm in diameter. The measurements were performed in such a way that the beam center was located 2.5 mm from the sample center. There a positron lifetime was obtained as the time between positron generation and its annihilation with an electron inside the sample. Mono-energetic positrons were accelerated to discrete energies (Ep) and implanted in the submicrometer region below the sample surface. After a short diffusion, positrons annihilate in delocalized states between atoms and/or localize in vacancy like defects and their agglomerations, which serve as a very attractive trap

for positrons. For the data acquisition a digital lifetime $CrBr_3$ scintillator detector was utilized, coupled to a Hamamatsu R13089-100 PMT. An in-house software employing a SPDevices ADQ14DC-2X digitizer with 14 bit vertical resolution and 2GS/s horizontal resolution [31] was used. The overall time resolution was better than about 0.240 ns. The resolution function required for spectrum analysis uses two Gaussian functions with distinct intensities depending on the positron implantation energy, E_p, and appropriate relative shifts. The typical lifetime spectrum N(t) is described by $N(t)=\Sigma\ (1/\tau_i)\ I_i\ \exp(-t/\tau_i)$, where τ_i and I_i are the positron lifetime and relative intensity of the i-th component, respectively ($\Sigma I_i=1$). All the spectra were deconvoluted, using PALSfit fitting software [32], into 3 discrete lifetime components, which directly evidence 2 different defect types (sizes). The 3rd component was neglected as a residual fingerprint of the surface ortho-Positronium (<0.5%). The corresponding relative intensities largely reflect the differences in concentration of each defect type (size). In general, the larger the open volume, the lower the probability and the longer it takes for positrons to be annihilated with electrons [33, 34].

c) Microstructure observations

Microstructure observations in the plan view, 0.5 and 3.5 from the sample center on samples prepared by conventional grinding, polishing and vibrating polishing, as described in the VEPALS analysis and methods section, were performed using a SU8000 Hitachi scanning electron microscope (SEM) at 5kV in the backscattered electron (BSE) mode. From the samples after HPT and combined HPT and HPA lamellae were cut 3.5 mm from the sample center, parallel to the radius beneath the sample surface, by a NB5000 Hitachi focused ion beam (FIB). The lamellae were then observed in bright field (BF) mode by transmission electron microscopy (TEM) using a JEOL 1200 at 120 kV. The microstructures obtained were further characterized by stereological and image analysis methods that are well-developed at the Warsaw University of Technology, Faculty of Materials Science and Engineering [35,36]. Calculations were then made of the average grain size (calculated as the equivalent diameter Avg (d_2)), the standard deviation of the equivalent diameter SD(d_2), and the variation coefficient of the equivalent diameter CV(d_2) which is the ratio of the standard deviation to the mean value.

d) Tensile tests

After conventional annealing, HPT and HPT combined with conventional annealing and HPA, uniaxial tensile tests were performed at RT using a Zwick/Roell Z005 machine. The

tensile tests were conducted under the displacement control mode at an initial strain rate of 10^{-3} s^{-1}. The dimensions of the samples were as follows: a gauge section length of 2 mm and a cross section of 0.3 mm × 0.4 mm. The strain measurements were performed using the digital image correlation method (DIC). After each tensile test, parameters such as ultimate tensile strength (UTS), yield stress (YS), uniform elongation (Au), and total elongation (At) were determined.

3. Results

3.1 Microhardness measurements

The microhardness measurements after various deformations and annealing treatment are presented in **Fig. 2.** After HPT, the microhardness increased from 97 to 324 Hv0.1. Subsequent annealing under pressure decreased the microhardness to an average value of 160 Hv0.1. However, when the pressure was maintained between the HPT and annealing, the average microhardness reached a slightly higher value of 189 Hv0.1. It is important to underline that the SD of the microhardness of the loaded sample was two times greater. Additionally, the microhardness was measured for HPA samples at 0.5 and 3.5 mm from the centre in order to verify what the impact of pressure was on a specific deformation degree. Similarly to the changes in the average microhardness values, the microhardness of the Ni_HPT_L_HPA was higher than for the Ni_HPT_U_HPA, at 178 and 149 Hv0.1, respectively, for 0.5 mm from the center and 205 and 175 Hv0.1, respectively, at 3.5 mm from the center.

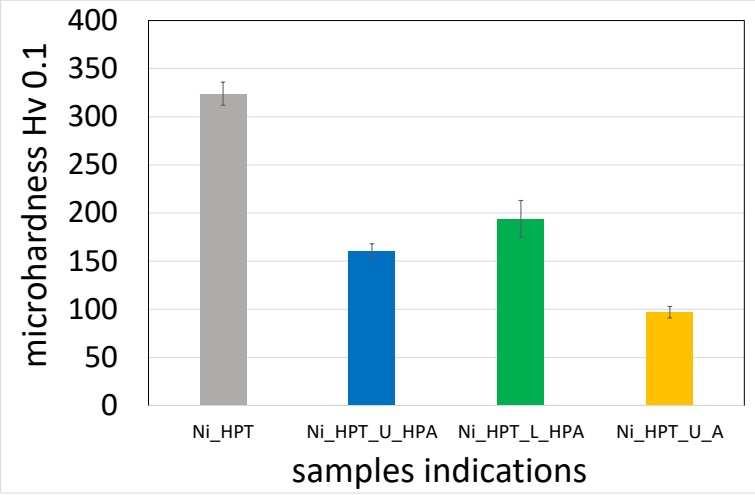

Fig. 2 Microhardness changes on the diameter of samples after various deformation and annealing treatments

3.2 Microstructure observations before HPA

Before the HPT experiments, Ni was annealed at 600°C for 2 h to homogenize its microstructure, as presented in **Fig. 3 a)**. After annealing, the average equivalent diameter was 31 μm. Subsequently, the HPT process was performed; it led to a refinement of grain size down to 140 nm on average (**Fig. 3 b)**). In the case of Ni_HPT microstructures are presented in the plan view and the cross section to enable the comparison in microstructures obtained by HPA.

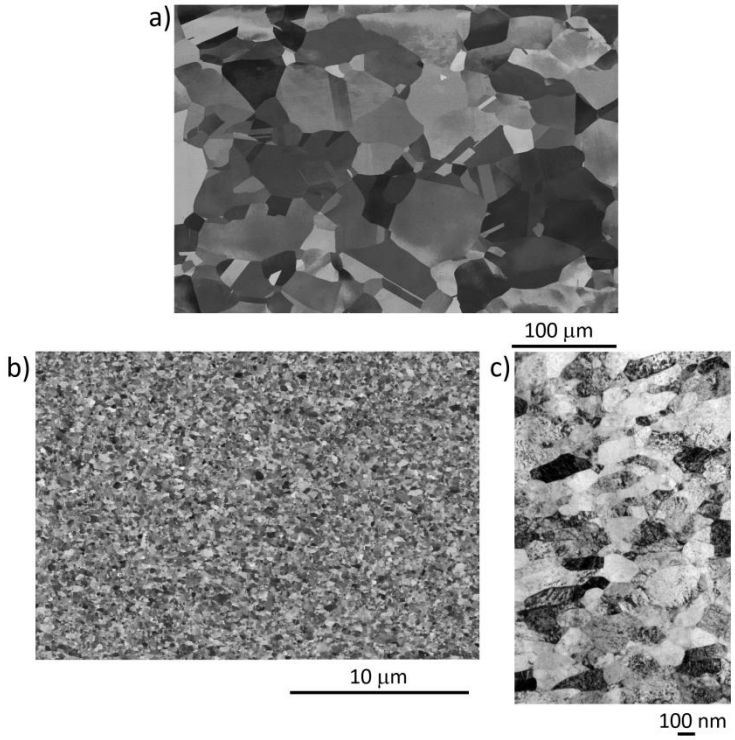

Fig. 3 Microstructures a) Ni_ A - plan view, b) Ni_HPT - plan view and c) Ni_HPT - cross section; a) and b) in BSE-mode, c) in BF-mode TEM

3.3 Defects characterisation after HPT

Fig. 4 shows a depth profile of positron lifetime components and their relative intensities of the Ni_HPT sample surface from the depth of ~220 nm. Due to the relatively large density of Ni and the depth probing limitations of the PALS setup, only a depth of <400 nm could be investigated (the maximum penetration by positrons is about 2×<z>). No reduced lifetime (no indication of positron annihilation at interatomic positions) was detected, which suggests a relatively large defect concentration. Spectra deconvolution leads to a positron lifetime τ_1 close to the literature value for Ni vacancy [37], but slightly lower, indicating mixed defect

states with dislocations (monovacancy-dislocation complexes)[38,39]. The second lifetime component τ_2 represents the superposition of surface states (E_p<7 keV) and vacancy clusters [40, 41]. One may expect to find vacancy clusters at grain boundaries, and the low intensity I_2 reflects their low density (a large overall size of crystallites). I_1 shows the tendency to increase with depth up to 95%, which reflects the decreasing signature of the surface and suggests that in the bulk material the main role is played by mono-vacancies associated with dislocations. These results are comparable with those obtained for HPT-processed Ni [41]. The large intensity of τ_1 suggests a large defect concentration, close to positron saturation trapping. The intensity of the component related to grain boundaries τ_2 is relatively low, which is in line with the general grain dimensions much larger than the positron diffusion length (estimated as not more than 20 nm). The fact that dislocations serve as positron traps in HPT-processed materials of relatively high melting temperature has been proved in the past [41].

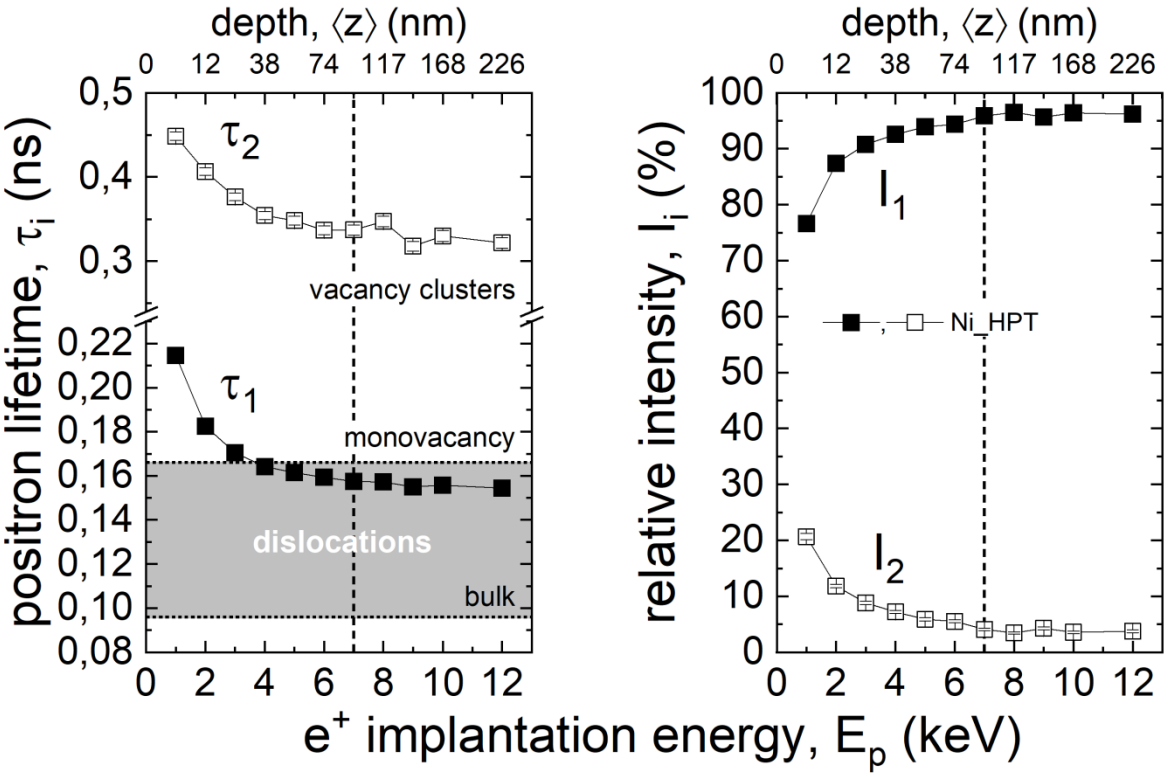

Fig. 4 Positron lifetime components τ_i and their relative intensities, I_i, as a function of positron implantation energy, E_p, and mean positron implantation depth, <z> for Ni_HPT. As a vertical line at E_p=7 keV the sub-surface border is given. The vertical lines and grey area show the lifetime ranges for bulk, dislocations and monovacancies [31].

3.4 Microstructure observations after HPT and subsequent HPA

The microstructures of the Ni samples after HPT and subsequent HPA with and without loading, observed 0.5 and 3.5 mm from the sample center, are presented in **Fig. 5**. The corresponding histograms of grain size distribution are shown in **Fig. 6**. The parameters characterising grain size and distribution are presented in **Table 1**. The results indicate that the loading between HPT and HPA had an impact on the microstructure transformation. Firstly, in the case of Ni_HPT_U_HPA, the average equivalent diameter was greater than for Ni_HPT_L_HPA. It equalled 1.3 and 0.88 μm at 0.5 mm, and 0.85 and 0.51 μm at 3.5 mm from the center, respectively. Moreover, loading led to a more heterogeneous microstructure in terms of grain size. This was well reflected by CV(d_2), which was higher for Ni_HPT_L_HPA than Ni_HPT_U_HPA by 100 and 20% at 0.5 mm and 3.5 mm from the center, respectively. It seems that when in-between loading is applied nearer the center, the number of grains of an equivalent diameter below 500 nm drops at the expense of grains greater than 2 μm.

Table 1 Average equivalent diameter d_2, standard deviation SD (d_2), and coefficient of variation CV(d_2) of grains in the Ni_HPT_U_HPA and Ni_HPT_L_HPA samples

Sample indication	Avg (d_2) [μm]	SD (d_2) [μm]	CV(d_2)
Ni_HPT_U_HPA – 0.5 mm from the centre	1.30	0.82	0.63
Ni_HPT_L_HPA– 0.5 mm from the centre	0.88	1.14	1.30
Ni_HPT_U_HPA– 3.5 mm from the centre	0.85	0.67	0.79
Ni_HPT_L_HPA– 3.5 mm from the centre	0.51	0.52	1.02

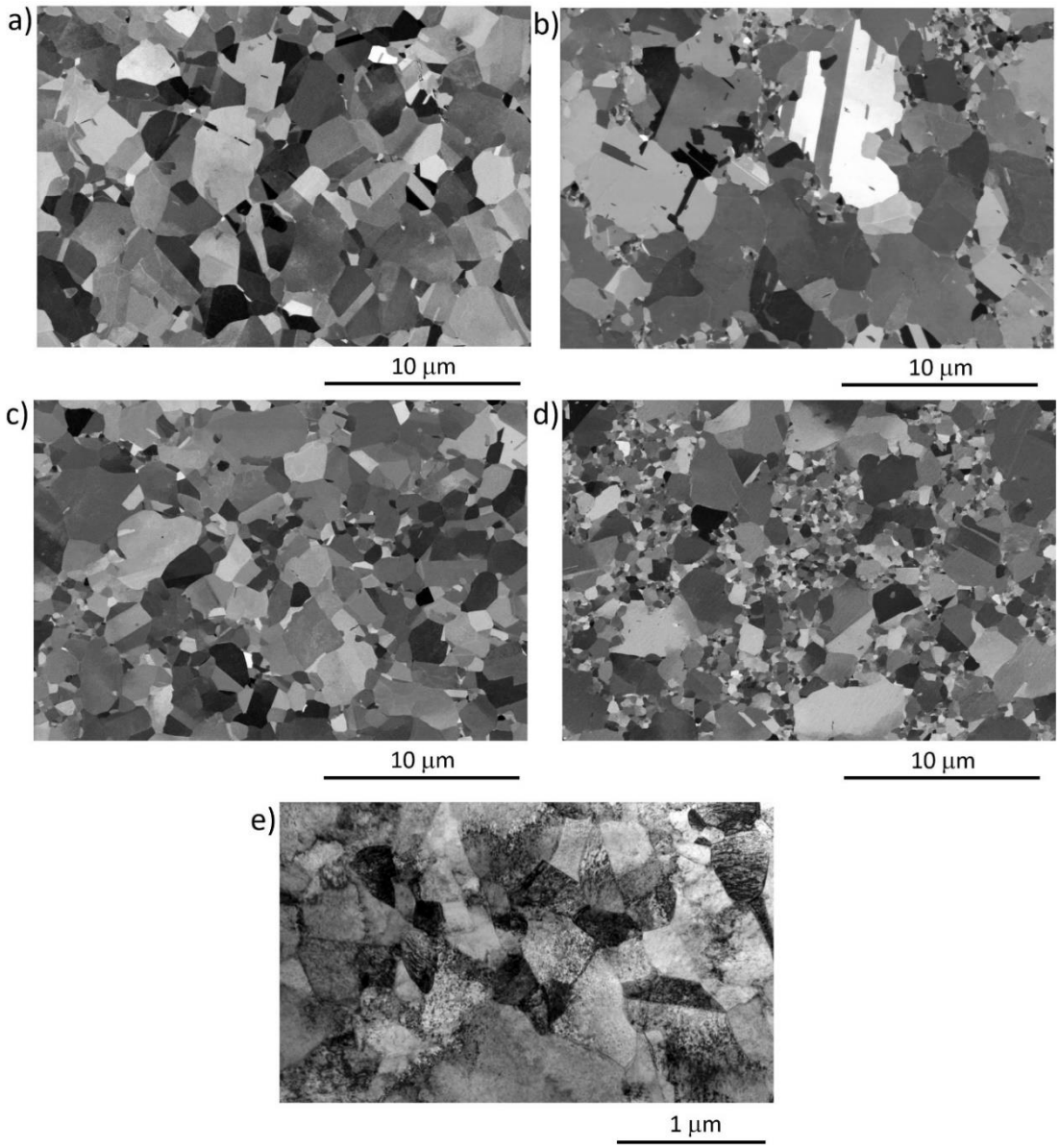

Fig. 5 Microstructures of Ni after HPT and subsequent HPA without a), c) and with b), d), e) loading after HPT; a)-d)-BSE-mode SEM, e) BF-mode TEM; a) and b) – 0.5 mm from the sample center, b), d, and e) – 3.5 mm from the sample center; a)-d) – plan view, e) cross section

a)

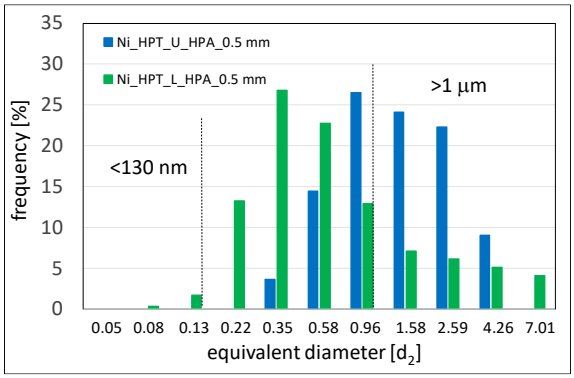

b)

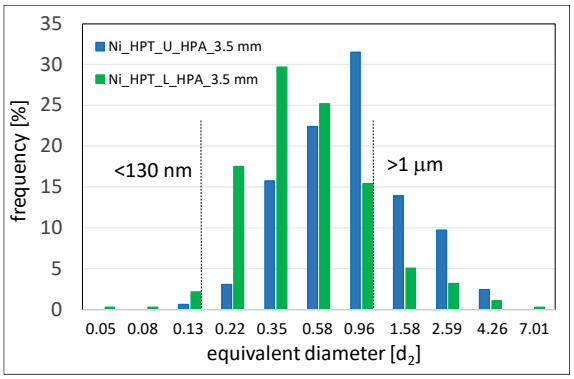

Fig. 6 Histograms of grain size distribution in Ni_HPT_L_HPA and Ni_HPT_U_HPA a) 0.5 mm and b) 3.5 mm from the sample center

3.5 Defects characterisation after HPA

Up to 100 nm below the surface, Ni_HPT, Ni_HPT_U_HPA and Ni_HPT_L_HPA are characterised by comparable defect types and concentrations, as presented in **Fig. 7 a)**. This phenomenon results from the surface preparation technique. However, approximately 100 nm below the surface one can clearly notice a difference between three samples. τ_1, representing monovacancy- dislocations complexes, has the highest intensity I_1 for Ni_HPT and the lowest for Ni_HPT_U_HPA. After HPA, τ_1 and I_1 slightly decreased, which indicates a reduction in the mono-vacancies associated with dislocations. For example, isolated threading dislocations are normally shallow positron traps [43] and require a complex with a monovacancy to be detectable at room temperature. After HPA, a change in vacancy cluster size is detected as well. In Ni_HPT_L_HPA, larger vacancy agglomerations are found than in Ni_HPT_U_HPA.

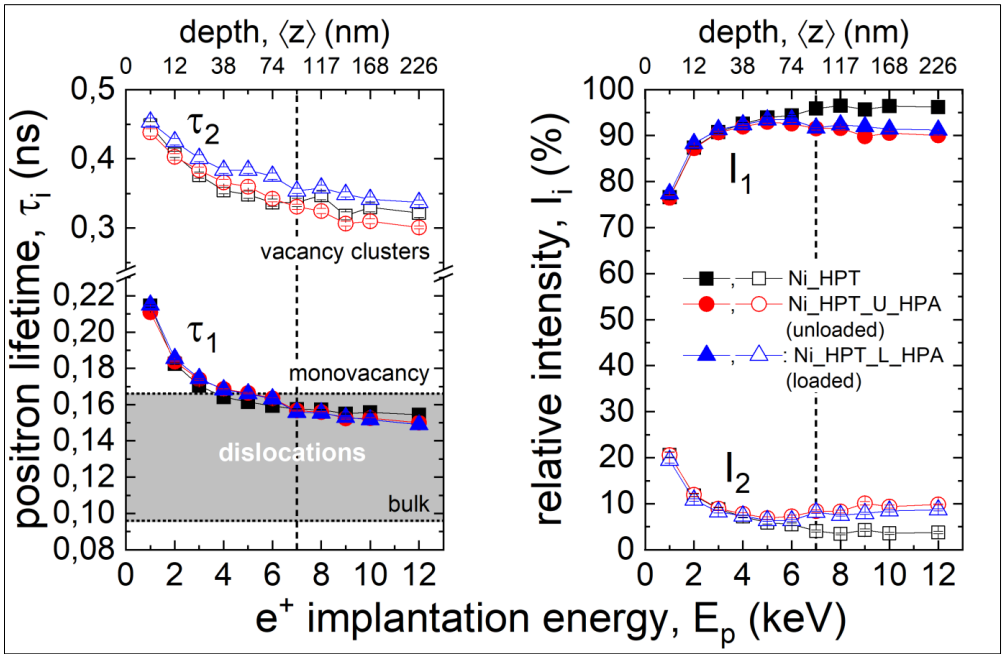

Fig. 7 Positron lifetime components τ_i and relative intensity, I_i, (a) as a function of positron implantation energy, E_p, and mean positron implantation depth, <z>, for Ni_HPT, Ni_HPT_U_HPA and Ni_HPT_L_HPA. The vertical line at E_p=7 keV represents a sub-surface border. The vertical lines and grey area show lifetime ranges for the bulk, dislocations and monovacancies [31]

3.6 Tensile tests

The stress–strain curves obtained during the room temperature tensile tests for Ni_HPT, Ni_HPT_L_HPA, Ni_HPT_U_HPA and Ni_A are presented in **Fig. 8**. The mean values (MV) and standard deviation (SD) of ultimate tensile strength (UTS), yield stress (YS), uniform elongation (Au), and total elongation (At) are summarized in **Table 2**.

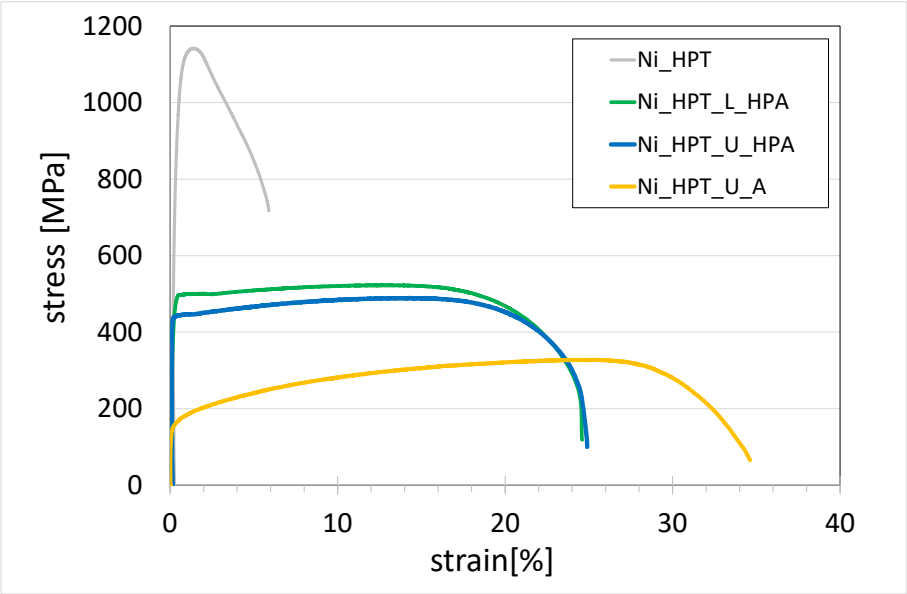

Fig. 8 Stress–strain curves obtained during room temperature tensile tests for Ni HPT-processed and annealed under various conditions

Table 2 MV and SD of UTS, YS, Au, and At for Ni HPT processed and annealed under various conditions

Parameter	YS [MPa]		UTS [MPa]		Au [%]		At [%]	
Sample indication	MV	SD	MV	SD	MV	SD	MV	SD
Ni_HPT	1049	6	1146	4	1.03	0.03	6.0	0.3
Ni_HPT_L_HPA	497	9	544	21	12.54	0.40	24.5	1.2
Ni_HPT_U_HPA	455	14	510	20	14.35	0.27	26.1	1.3
Ni_HPT_U_A	171	15	349	21	26.0	0.6	35.2	0.6

The results indicate that HPT increased the UTS from 349 after annealing to 1146 MPa. This value is in between the values reported in the literature, i.e. 1270 MPa [27] and 1015 MPa [43]. The results show that the loading applied between the HPT and HPA led to an increase in strength with a slight decrease in plasticity in comparison with Ni_HPT_U_HPA. This phenomenon can be explained by the greater volume of ultrafine grains in Ni_HPT_L_HPA than in Ni_HPT_U_HPA, which are responsible for higher strength.

It seems that by the proper selection of temperature and annealing pressure and with the application of loading between deformation and annealing, microstructures consisting of nanograins and micrograins of high strength (nanograins) and satisfactory ductility

(micrograins) can be obtained. Creating such microstructures is one of the approaches that have been successfully applied to increase the plasticity of nanostructured and ultrafine grained materials [44].

4. Discussion

4.1 The impact of loading after HPT on microstructure transformation during HPA

Materials produced by SPD are usually less thermally stable than conventionally deformed materials because they have a higher stored energy in the form of lattice defects. The high hydrostatic pressure typical of HPT can increase the concentration of vacancies due to the limited atomic mobility that exists under such conditions. Therefore, during annealing after HPT, the atomic diffusion is enhanced significantly, since it is directly proportional to the concentration of vacancies [45]. Some SPD-processed materials can even exhibit self-annealing due to their stored energy and to their low melting temperature, which can accelerate recrystallization and grain growth [46,47].

Moreover, it is important to add that in SPD-processed materials some grain boundaries are what is known as ‘non-equilibrium’ grain boundaries. Non-equilibrium grain boundaries are specific grain boundaries that are characterized by an increased free energy that is the result of a high density of defects such dislocations and vacancies, and consequently high residual microstrains [48]. These boundaries are characterised by enhanced diffusivity, which in turn can enhance grain growth. In SPD-processed pure fcc metals, the activation energy of recovery/recrystallization is approximately 0.5±0.1 of self-diffusion, which well-corresponds with the value of activation energy of diffusion along grain boundaries and dislocations [49-51].

As expected, the thermal stability of the SPD-processed Ni was lower than that of the conventionally deformed material [52]. Previous experiments have shown that additional pressure during annealing - 2GPa at 400°C for 1 h - slowed down grain growth in HPT-processed Ni in comparison with atmospheric pressure annealing, so that the grain size after HPA reached approximately 70% of the grain size after conventional annealing [27]. Moreover, the process also affected the homogeneity of the microstructures by significantly increasing CV(d_2) [27]. This study proved that additional loading between deformation and annealing made it possible to preserve some of the vacancies generated during HPT - some, not all, since the HPT was performed at a pressure of 6GPa and the HPA at a pressure of

2GPa. The fact that in Ni_HPT_L_HPA the concentration of representing monovacancy-dislocations complexes was slightly higher than in Ni_HPT_U_HPA was confirmed by the VEPALS measurements. Moreover, the applied loading made the migration of released vacancies to grain boundaries difficult, so some of them might have agglomerated, creating larger vacancy clusters than those in Ni_HPT_U_HPA, as proved by the VEPALS, too. This means that, even though the vacancy concentration was higher in the loaded sample during HPA than in the unloaded sample, their migration to defect sinks, which in the case of HPT-processed materials are mainly grain boundaries and dislocations, was limited [53]. As a result, the migration of grain boundaries was hindered, and Ni_HPT_L_HPA was characterized by a smaller average equivalent diameter than Ni_HPT_U_HPA.

It is also interesting that a more heterogeneous microstructure was created in Ni_HPT_L_HPA than in Ni_HPT_U_HPA. The fact that abnormal grain growth occurred in Ni_HPT_L_HPA can be deduced from the microstructure images, since abnormal grains exhibit a high twin density, likely due to an increased grain boundary migration rate [54]. It might be that the distribution of vacancies within boundaries is orientation-dependent, combined with the presence of orientation gradients that promote selective grain growth [55]. Moreover, it may also result from the presence of some percentage of low-angle grain boundaries in the HPT-processed Ni [4]. Low-angle grain boundaries migrate only by the vacancy migration mechanism [20], which is strongly limited during HPA. For this reason, in such areas grain growth can be restricted.

4.2 The impact of strain on the microstructure transformation during HPA

This study made it possible to observe that the greater the strain, and the further from the sample centre, in the case of Ni_HPT_U_HPA and Ni_HPT_L_HPA the smaller the average grain size after annealing. The significantly enhanced thermal stability for higher strains is an interesting phenomenon, since during annealing under atmospheric pressure the inverse behaviour is usually observed. In Ag, Au and Cu after HPT kept at room temperature for a long time, the softening becomes more significant as the distance from the disc center increases [46]. However, the significantly enhanced thermal stability for higher strains in this study may be justified by the faster recovery of non-equilibrium grain boundaries under pressure for higher strains due to their enhanced diffusivity, as mentioned in [56]. The fact

that materials deformed to higher strains show greater thermal stability than materials deformed to lower strains was also revealed on the example of profile-rolled (PR) and HPT-processed austenitic stainless steel. In the former case, after conventional annealing for 10 min at 900°C, grain growth was enhanced. This was due to the fact that the microstructure of PR-processed steel was heterogeneous, which means there were preferred sites for the formation of nuclei having high local misorientations. In the case of HPT-processed austenitic stainless steel, normal grain growth was observed [22]. A similar phenomenon can also be observed in this study. After HPT, the higher the strains, the more refined and homogenous the microstructure [57], while homogeneity promotes slower grain growth under pressure. This is achieved because there is limited atomic mobility of vacancies under high pressure.

Conclusions

1. Additional loading under 2GPa between deformations by HPT under 6GPa and HPA under 6GPa at 400°C for 5min causes an increase in microhardness by 20% in comparison with no loading applied.
2. Additional loading under 2GPa between deformation by HPT under 6GPa and HPA under 6GPa at 400°C leads to a smaller average equivalent diameter and a more heterogenous microstructure in terms of grain size in comparison with no loading applied. Moreover, it leads to a higher concentration of representing monovacancy-dislocations complexes and larger vacancy clusters in comparison with no loading applied.
3. The greater the strain, the smaller the grain size after HPA since there is limited atomic mobility under pressure in the homogeneous areas of samples.
4. Additional pressure between HPT and HPA may be successfully applied to modify the microstructure and obtain an optimised strength-plasticity balance.

Acknowledgements

Parts of this research were carried out at ELBE at the Helmholtz-Zentrum Dresden - Rossendorf e. V., a member of the Helmholtz Association. We would like to thank the facility staff for assistance, especially Ahmed G. Attallah.

The raw/processed data required to reproduce these findings cannot be shared at this time due to technical or time limitations.

References

1. R.Z. Valiev, R.K. Islamgaliev, I. V. Alexandrov, Bulk nanostructured materials from severe plastic deformation, Prog. Mater. Sci. (2000). doi:10.1016/S0079-6425(99)00007-9.
2. Y.T. Zhu, T.G. Langdon, The fundamentals of nanostructured materials processed by severe plastic deformation, JOM. (2004). doi:10.1007/s11837-004-0294-0.
3. R.Z. Valiev, Y. Estrin, Z. Horita, T.G. Langdon, M.J. Zehetbauer, Y.T. Zhu, Producing bulk ultrafine-grained materials by severe plastic deformation, JOM. (2006). doi:10.1007/s11837-006-0213-7.
4. X. Sauvage, G. Wilde, S. V. Divinski, Z. Horita, R.Z. Valiev, Grain boundaries in ultrafine grained materials processed by severe plastic deformation and related phenomena, Mater. Sci. Eng. A. 540 (2012) 1–12. doi:10.1016/j.msea.2012.01.080.
5. X.H. An, S.D. Wu, Z.G. Wang, Z.F. Zhang, Significance of stacking fault energy in bulk nanostructured materials: Insights from Cu and its binary alloys as model systems, Prog. Mater. Sci. (2019). doi:10.1016/j.pmatsci.2018.11.001.
6. Y.B. Wang, J.C. Ho, Y. Cao, X.Z. Liao, H.Q. Li, Y.H. Zhao, E.J. Lavernia, S.P. Ringer, Y.T. Zhu, Dislocation density evolution during high pressure torsion of a nanocrystalline Ni-Fe alloy, Appl. Phys. Lett. (2009). doi:10.1063/1.3095852.
7. E. Schafler, G. Steiner, E. Korznikova, M. Kerber, M.J. Zehetbauer, Lattice defect investigation of ECAP-Cu by means of X-ray line profile analysis, calorimetry and electrical resistometry, Mater. Sci. Eng. A. (2005). doi:10.1016/j.msea.2005.08.070.
8. D. Setman, E. Schafler, E. Korznikova, M.J. Zehetbauer, The presence and nature of vacancy type defects in nanometals detained by severe plastic deformation, Mater. Sci. Eng. A. 493 (2008) 116–122. doi:10.1016/j.msea.2007.06.093.
9. J. Čížek, M. Janeček, O. Srba, R. Kužel, Z. Barnovská, I. Procházka, S. Dobatkin, Evolution of defects in copper deformed by high-pressure torsion, Acta Mater. (2011). doi:10.1016/j.actamat.2010.12.028.
10. J. Čížek, O. Melikhova, M. Janeček, O. Srba, Z. Barnovská, I. Procházka, S. Dobatkin, Homogeneity of ultrafine-grained copper deformed by high-pressure torsion characterized by positron annihilation and microhardness, Scr. Mater. (2011). doi:10.1016/j.scriptamat.2011.04.006.

11. P. Cengeri, M.B. Kerber, E. Schafler, M.J. Zehetbauer, D. Setman, Strengthening during heat treatment of HPT processed copper and nickel, Mater. Sci. Eng. A. (2019). doi:10.1016/j.msea.2018.11.010.
12. M.J. Zehetbauer, H.P. Stüwe, A. Vorhauer, E. Schafler, J. Kohout, The role of hydrostatic pressure in severe plastic deformation, Adv. Eng. Mater. (2003). doi:10.1002/adem.200310090.
13. M. Kerber, F. Spieckermann, R. Schuster, B. Joni, N. Schell, E. Schafler, In-situ synchrotron profile analysis after high-pressure torsion deformation, Crystals. (2019). doi:10.3390/cryst9050232.
14. E. Schafler, Strength response upon pressure release after high pressure torsion deformation, Scr. Mater. (2011). doi:10.1016/j.scriptamat.2010.09.026.
15. E. Schafler, Effects of releasing the hydrostatic pressure on the nanostructure after severe plastic deformation of Cu, Scr. Mater. (2010). doi:10.1016/j.scriptamat.2009.12.004.
16. W. Lojkowski, D.A. Molodov, G. Gottstein, L.S. Shvidlerman The mechanism of grain boundary migration in aluminium bicrystals. Mater Sci Forum (1996) 207–209:537–540.
17. L.S. Shvindlerman, U. Czubayko, G. Gottstein, D. A. Molodov High pressure effect on grain boundary migration and mechanism of grain boundary migration. Mater Sci Forum (1996) 204–206:45–54.
18. A.F. Syrenko, G. P. Klinishev, V. T. Khoi: Recrystallization of copper under hydrostatic pressure up to 15kbar, J Mater Sci 8 (1973) 765-769.
19. L.E. Tanner, S. V. Radcliffe: Effect of hydrostatic pressure on the kinetics of recrystallization in high-purity copper, Acta Metall Mater 10 (1962) 1161-1169.
20. V. Sursaeva, S. Protasova, W. Lojkowski, J. Jun, Microstructure Evolution During Normal Grain Growth Under High Pressure in 2-D Aluminium Foils, Textures Microstruct. (2008). doi:10.1155/tsm.32.175.
21. A.T. Krawczynska, T. Brynk, S. Gierlotka, E. Grzanka, S. Stelmakh, B. Palosz, M. Lewandowska, K.J. Kurzydlowski, Mechanical properties of nanostructured 316LVM stainless steel annealed under pressure, Mech. Mater. (2013). doi:10.1016/j.mechmat.2013.07.017.
22. A.T. Krawczynska, S. Gierlotka, P. Suchecki, D. Setman, B. Adamczyk-Cieslak, M. Lewandowska, M. Zehetbauer, Recrystallization and grain growth of a nano/ultrafine

structured austenitic stainless steel during annealing under high hydrostatic pressure, J. Mater. Sci. (2018). doi:10.1007/s10853-018-2459-1

23. A.T. Krawczynska, S. Gierlotka, P. Suchecki, D. Setman, B. Adamczyk-Cieslak, M. Gloc, W. Chrominski, M. Lewandowska, M. Zehetbauer, Phenomena Occurring in Nanostructured Stainless Steel 316LVM during Annealing under High Hydrostatic Pressure, Adv. Eng. Mater. (2018). doi:10.1002/adem.201800101
24. A.T. Krawczynska, P. Suchecki, B. Adamczyk-Cieslak, B. Romelczyk-Baishya, M. Lewandowska, Influence of high hydrostatic pressure annealing on the recrystallization of nanostructured austenitic stainless steel, Mater. Sci. Eng. A. (2019). doi:10.1016/j.msea.2019.138381.
25. A.T. Krawczynska, M. Lewandowska, R. Kuziak, K.J. Kurzydłowski, Recrystallization and grain growth in nano-structured austenitic stainless steel under electric current heating, Phys. Status Solidi. (2010). doi:10.1002/pssc.200983377
26. A.T. Krawczynska, T. Brynk, M. Rosioski, A. Michalski, S. Gierlotka, E. Grzanka, S. Stelmakh, B.Pałosz, M. Lewandowska, K.J. Kurzydłowski, Improving mechanical properties of nanometals by annealing, Proceedings of The 33rd Risoe International Symposium on Materials Science:Nanometals - Status and Perspective, (2012) 279-286.
27. A.T. Krawczynska, M. Kerber, P. Suchecki, B. Romelczyk-Baishya, M. Lewandowska, D. Setman, The impact of the stacking fault energy of nanostructured metals on phenomena during annealing at the high hydrostatic pressure, Mater. Sci. Eng. A. (2021). doi:10.1016/j.msea.2021.140913.
28. P.C.J. Gallagher, The influence of alloying, temperature and related effects on the stacking fault energy, Metall. Trans. 1 (1970) 2429–2461
29. A. Wagner, W. Anwand, A.G. Attallah, G. Dornberg, M. Elsayed, D. Enke, A.E.M. Hussein, R. Krause-Rehberg, M.O. Liedke, K. Potzger, T.T. Trinh, Positron annihilation lifetime spectroscopy at a superconducting electron accelerator, J. Phys. Conf. Ser. 791 (2017) 012004. doi.org/10.1088/1742-6596/791/1/012004.
30. A. Wagner, M. Butterling, M.O. Liedke, K. Potzger, R. Krause-Rehberg, Positron annihilation lifetime and Doppler broadening spectroscopy at the ELBE facility, in: AIP Conf. Proc., 2018: p. 040003. doi.org/10.1063/1.5040215.
31. E. Hirschmann, M. Butterling, U. Hernandez Acosta, M.O. Liedke, A.G. Attallah, P. Petring, M. Görler, R. Krause-Rehberg, A. Wagner, A new system for real-time data acquisition and pulse parameterization for digital positron annihilation lifetime

spectrometers with high repetition rates, J. Instrum. 16 (2021) P08001. https://doi.org/10.1088/1748-0221/16/08/P08001.

32. J. V. Olsen, P. Kirkegaard, N.J. Pedersen, M. Eldrup, PALSfit: A new program for the evaluation of positron lifetime spectra, Phys. Status Solidi. 4 (2007) 4004–4006. doi.org/10.1002/pssc.200675868.
33. R. Krause-Rehberg, H.S. Leipner, Positron annihilation in semiconductors: defect studies, 1999.
34. F. Tuomisto, I. Makkonen, Defect identification in semiconductors with positron annihilation: Experiment and theory, Rev. Mod. Phys. 85 (2013) 1583–1631. doi.org/10.1103/revmodphys.85.1583.
35. T. Wejrzanowski, W.L. Spychalski, K. Rózniatowski, K.J. Kurzydłowski, Image based analysis of complex microstructures of engineering materials, Int. J. Appl. Math. Comput. Sci. (2008). doi:10.2478/v10006-008-0003-1.
36. T. Wejrzanowski, K.J. Kurzydlowski, K.J. Stereology of grains in nano-crystals , Solid State Phenomena 94 (2003) pp. 221-228
37. J.M.C. Robles, E. Ogando, F. Plazaola, Positron lifetime calculation for the elements of the periodic table, J. Phys. Condens. Matter. 19 (2007) 176222. doi.org/10.1088/0953-8984/19/17/176222.
38. J. Čížek, O. Melikhova, Z. Barnovská, I. Procházka, R.K. Islamgaliev, Vacancy clusters in ultra fine grained metals prepared by severe plastic deformation, J. Phys. Conf. Ser. 443 (2013) 012008. doi.org/10.1088/1742-6596/443/1/012008.
39. L.C. Smedskjaer, M. Manninen, M.J. Fluss, An alternative interpretation of positron annihilation in dislocations, J. Phys. F Met. Phys. 10 (1980) 2237–2249. doi.org/10.1088/0305-4608/10/10/019.
40. T. Yoshiie, M. Hasegawa, S. Kojima, K. Sato, Y. Saitoh, S. Yamaguchi, M. Kiritani, Positron lifetime measurement and latent vacancy clusters in 14 MeV neutron irradiated nickel, J. Nucl. Mater. 179–181 (1991) 931–934. doi.org/10.1016/0022-3115(91)90242-Y.
41. J. Čížek, M. Janeček, T. Vlasák, B. Smola, O. Melikhova, R.K. Islamgaliev, S. V. Dobatkin, The development of vacancies during severe plastic deformation, Mater. Trans. (2019). doi:10.2320/matertrans.MF201937.
42. S. Assali, M. Elsayed, J. Nicolas, M.O. Liedke, A. Wagner, M. Butterling, R. Krause-Rehberg, O. Moutanabbir, Vacancy complexes in nonequilibrium germanium-tin semiconductors, Appl. Phys. Lett. 114 (2019) 112–117. doi:10.1063/1.5108878.

43. A.P. Zhilyaev, S. Lee, G.V. Nurislamova, R.Z. Valiev, T.G. Langdon, Microhardness and microstructural evolution in pure nickel during high-pressure torsion, Scripta Mater. (2001), 10.1016/S1359-6462(01)00955-1.
44. Y.M. Wang, E. Ma, Three strategies to achieve uniform tensile deformation in a nanostructured metal, Acta Mater. 52 (2004) 1699–1709. doi:10.1016/j.actamat.2003.12.022.
45. H. Mehrer, Numerical Data and Functional Relationship in Science and TechnologyVol. 26 Diffusion in Solid Metals and Alloys, Springer, Berlin, 1990.
46. K. Edalati, Y. Hashiguchi, H. Iwaoka, H. Matsunaga, R.Z. Valiev, Z. Horita, Long-time stability of metals after severe plastic deformation: Softening and hardening by self-annealing versus thermal stability, Mater. Sci. Eng. A. 729 (2018) 340–348. doi:10.1016/j.msea.2018.05.079.
47. Z. Hegedus, J. Gubicza, P. Szommer, N.Q. Chinh, Y. Huang, T.G. Langdon, Inhomogeneous softening during annealing of ultrafine-grained silver processed by HPT, J. Mater. Sci. 48 (2013) 7384–7391. doi:10.1007/s10853-013-7553-9.
48. X. Sauvage, G. Wilde, S. V. Divinski, Z. Horita, R.Z. Valiev, Grain boundaries in ultrafine grained materials processed by severe plastic deformation and related phenomena, Mater. Sci. Eng. A. 540 (2012) 1–12. doi:10.1016/j.msea.2012.01.080.
49. C.M. Kuo, C.S. Lin, Static recovery activation energy of pure copper at room temperature, Scr. Mater. 57 (2007) 667–670. doi:10.1016/j.scriptamat.2007.06.054.
50. J. Lian, R.Z. Valiev, B. Baudelet, On the enhanced grain growth in ultrafine grained metals, Acta Metall. Mater. 43 (1995) 4165–4170. doi:10.1016/0956-7151(95)00087-C.
51. G. Kapoor, Y. Huang, V. Subramanya Sarma, T.G. Langdon, J. Gubicza, Evolution of the microstructure during annealing of ultrafine-grained Ni with different Mo contents, Mater. Charact. 130 (2017) 56–63. doi:10.1016/j.matchar.2017.05.034.
52. Zhilyaev, A.P., Nurislamova, G.V., Valiev, R.Z. et al. Thermal stability and microstructural evolution in ultrafine-grained nickel after equal-channel angular pressing (ECAP). Metall Mater Trans A 33, 1865–1868 (2002). doi.org/10.1007/s11661-002-0197-z
53. R. Enzinger, C. Neubauer, J. Kotzurek, W. Sprengel, R. Würschum, Kinetics of vacancy annealing upon time-linear heating applied to dilatometry, J. Mater. Sci. (2018). doi:10.1007/s10853-017-1780-4.
54. C.S. Pande, M.A. Imam, B.B. Rath, Study of annealing twins in FCC metals and

alloys, Metall. Trans. A, Phys. Metall. Mater. Sci. 21 A (1990) 2891–2896. doi:10.1007/BF02647209.

55. S. Bunkholt, E. Nes, K. Marthinsen, Orientation independent and dependent subgrain growth during iso-thermal annealing of high- purity and commercial purity aluminium, Metals (Basel). 9 (2019) 1–19. doi:10.3390/met9101032.
56. R. Z. Valiev, Paradoxes of Severe Plastic DeformationAdvanced Engineering Materials 5 (2003), doi-1org-10000abe6014d.eczyt.bg.pw.edu.pl/10.1002/adem.200310089
57. A. Vorhauer, R. Pippan, On the homogeneity of deformation by high pressure torsion, Scr. Mater. 51 (2004) 921–925. doi:10.1016/j.scriptamat.2004.04.025.